

Structural Details of Human Tuba Recruitment by InIC of *Listeria monocytogenes* Elucidate Bacterial Cell-Cell Spreading

Lilia Polle^a, Luciano Rigano^b, Rowan Julian^a, Keith Ireton^b and Wolf-Dieter Schubert^{a,c,#}

^a Department of Biotechnology, University of the Western Cape, Bellville 7535, Cape Town, South Africa, ^b Department of Microbiology and Immunology, University of Otago, Dunedin 9054, New Zealand, ^c Department of Biochemistry, University of Pretoria, Pretoria 0002, South Africa, [#] Corresponding author: Phone: +27-12-420-6987, E-mail: wolf-dieter.schubert@up.ac.za

Summary

The human pathogen *Listeria monocytogenes* is able to directly spread to neighboring cells of host tissues, a process recently linked to the virulence factor InlC. InlC targets the sixth SH3 domain (SH3-6) of human Tuba, disrupting its physiological interaction with the cytoskeletal protein N-WASP. The resulting loss of cortical actin tension proposedly slackens the junctional membrane allowing protrusion formation by motile *Listeria*. Complexes of Tuba SH3-6 with physiological partners N-WASP and Mena reveal equivalent binding modes but distinct affinities. The interaction surface of the infection complex InlC/Tuba SH3-6 is centered on phenylalanine146 of InlC stacking upon asparagine1569 of Tuba. Replacing Phe146 by alanine largely abrogates molecular affinity and *in vivo* mimics deletion of *inlC*. Collectively, our findings indicate that InlC hijacks Tuba through its LRR domain, blocking the peptide binding groove to prevent recruitment of its physiological partners.

Keywords: Molecular mechanism of infection, engineering of protein-protein interactions, LRR proteins

Introduction

The food-borne pathogen *Listeria monocytogenes* (*Lm*), an important Gram positive model organism, opportunistically infects immuno-compromised individuals, pregnant women, and newborns (Hamon et al., 2006; Cossart, 2007; Schlech, III, 2000). Listerial virulence critically depends on bacteria spreading from infected host cells to surrounding healthy cells avoiding antibody-mediated immunity (Vazquez-Boland et al., 2001; Cossart, 2007). The listerial surface protein ActA assembles host actin filaments into tail-like structures to propel bacteria through the cytosol (Welch et al., 1997). On contact with the host cell membrane, motile *Listeria* form membrane protrusions that may be engulfed by neighboring human cells.

Protrusion formation and cell spreading are dependent on the secreted bacterial virulence factor InlC (Rajabian et al., 2009) required for full virulence in mice (Engelbrecht., 1996; Gouin et al., 2010) and cell spread in the liver (Leung et al., 2013). Deletion of *inlC* does not affect motility, implying InlC and ActA act independently.

InlC is the only secreted member of the internalin family of proteins typical of pathogenic *Lm* and *L. ivanovii*. It consists exclusively of the fused internalin domain comprising an N-terminal cap, a central leucine-rich repeat (LRR) and a C-terminal immunoglobulin-like domain (Engelbrecht., 1996; Ooi et al., 2006; Schubert et al., 2001). InlC targets both human IKK α , to interfere with the immune response to invading pathogens (Gouin et al., 2010) and human Tuba to promote the *Lm* cell spreading (Rajabian et al., 2009).

Cytosolic Tuba (180 kDa) comprises six Src Homology 3 (SH3) domains, a lipid-binding Bin–amphiphysin–Rvs (BAR) domain, and a Dbl homology (DH) domain with guanine nucleotide exchange activity for human GTPase Cdc42 (Salazar et al., 2003). Its four N-terminal SH3 domains bind human dynamin I. The ligand of the fifth SH3 domain is unknown. The sixth or C-terminal SH3 domain (SH3-6) of Tuba binds proline-rich regions of human actin regulatory proteins, such as N-WASP and Mena (Salazar et al., 2003). By targeting Tuba, InlC displaces N-WASP, affecting cortical tension and slackening cell junctions to allow more facile protrusion formation and hence *Lm* cell-cell spread (Rajabian et al., 2009). Only indirect data exist for InlC recognition of Tuba SH3-6 and how physiological Tuba function is affected. Despite structural data for InlC and SH3 domains, *in silico* prediction of molecular interaction remains too imprecise for detailed functional analysis (Pons et al., 2010). To elucidate this critical interaction with high precision we have undertaken a detailed structural and biophysical characterization combined with cell-based analyses. We present crystal structures of Tuba SH3-6 in complex with N-WASP and Mena peptides and the complex of Tuba SH3-6 and InlC. InlC is seen to physically block the

binding groove of Tuba SH3-6 displacing the proline-rich partners. InlC/Tuba SH3-6 interaction is centered on Phe146^{InlC} stacking on Asn1569^{Tuba}. Replacing Phe146^{InlC} by alanine abrogates binding of Tuba SH3-6 *in vitro*. A corresponding listerial mutant mimics *inlC* deletion in showing reduced protrusion formation and cell-cell spread. Our work thus confirms the direct interaction of InlC and Tuba SH3-6, elucidating the details of molecular recognition as well as the mechanism by which InlC is able to displace host binding proteins from Tuba to promote cell-cell spread.

Results

Crystal structure of Tuba SH3-6 binding proline-rich peptides

Crystal structures of Tuba SH3-6 (residues 1513-1577, dark green, Figure 1 a) in complex with 12-residue, proline-rich peptides from human N-WASP (³⁴⁶PPPALPSSAPSG³⁵⁷, red) and murine Mena (⁵⁴⁷PPPPLPSGPAYA⁵⁵⁸, yellow) (Table 1) reveal a typical SH3 domain fold comprising an antiparallel, five-stranded β -barrel with a 3_{10} -helix in loop β 4- β 5. N- and C-termini of Tuba SH3-6 are flexible and adopt distinct conformations. Both peptides form polyproline type II (PPII) helices and bind in a class II orientation (Lim et al., 1994). The contact surface area of Tuba SH3-6 with N-WASP and Mena peptides is $\sim 500 \text{ \AA}^2$ ($\sim 10\%$ of total). Residues in the peptide-binding groove between RT-Src (β 1- β 2) and n-Src (β 3- β 4) loops, conserved in SH3 domains (Larson and Davidson, 2000) are shown in blue (Figure 1b). Other residues critical for peptide recognition are in grey. All central residues of the proline-rich peptides interact with Tuba SH3-6 amounting to $\sim 600 \text{ \AA}^2$ ($\sim 44\%$). Complex formation between Tuba SH3-6 and the proline-rich peptides was investigated by isothermal titration calorimetry (ITC) (Figure 1 c). Dissociation constants for N-WASP and Mena are $46.5 \pm 5 \text{ \mu M}$ and $72.5 \pm 24 \text{ \mu M}$, respectively, similar to other SH3 domain/peptide interactions (Alexandropoulos et al., 1995; Sparks et al., 1996).

InlC/Tuba SH3-6 complex structure

InlC (residues 35-297)/Tuba SH3-6 crystals were obtained after replacing Tyr246 and Tyr247 of InlC by alanine to prevent InlC-only crystals. The InlC/Tuba SH3-6 crystal structure reveals three 1:1 complexes per asymmetric unit that concur with respect to the interaction mode (Figure 2 b). Noticeable differences in the three complexes indicate some plasticity near the periphery of the interaction. For InlC, essentially unchanged from its ligand-free form (Ooi et al., 2006), differences are limited to side chain conformations. In Tuba SH3-6, the β -barrel core reveals only minimal InlC-induced perturbations compared to the N-WASP and Mena complexes. The peptide-binding RT- and n-Src loops, by contrast, show some variation (Figure 2 b). Similarly, the N- and C-termini, prior to the first and following the last β -strands, adopt distinct conformations (Figure 2 b). AS termini are individually well resolved, differences are not due to disorder. We limited our analyses to invariant InlC/Tuba SH3-6 complex features, discussing minority conformations only where relevant (Table S2).

The InlC/Tuba SH3-6 interaction involves only $\sim 520 \text{ \AA}^2$ or 4% of the solvent-accessible surface of InlC (Figure 2 c, blue) and 570 \AA^2 (12%) of Tuba SH3-6 (green). InlC binds Tuba SH3-6 via its concave LRR surface (Figure 2 a): each β -strand plus adjoining loops contributes from one to three interacting residues (Figure 3 a, c, Table S2). LRRs 1 and 2, and Arg128 of LRR3 contact the Tuba SH3-6 n-Src loop. LRRs 3 to 7 interact with the N-terminal residues of the RT-Src loop, the 3_{10} -helix and β -strand 5. Lys173^{InlC}, postulated to be part of a Tuba SH3-6 RXXK decoy motif (Rajabian et al., 2009; Leung et al., 2013), is unexpectedly not involved in the InlC/Tuba SH3-6 interaction (Figure 2 c).

The central interaction of the InlC/Tuba SH3-6 recognition involves Phe146^{InlC} stacking upon Asn1569^{Tuba} (3_{10} -helix, Figure 3 a) plus van der Waals contacts to Tyr1570^{Tuba}. Asn1569^{Tuba} also hydrogen bonds Ser125^{InlC}, Asn127^{InlC} and Asp148^{InlC}, while Tyr1570^{Tuba} hydrogen bonds Glu123^{InlC}. The guanido group of Arg144^{InlC} extensively stacks upon Tyr1522^{Tuba}. In

one of three complexes, Tyr1522^{Tuba} rotates slightly around chi1 creating a hydrogen bond to Glu1651^{InlC} and van der Waals contacts to Arg144^{InlC}. Arg1572^{Tuba}, showing some variation in conformation, invariably engages Ser168^{InlC} and Asp190^{InlC} through a hydrogen bond/salt bridge and forms a C-H... π interaction with Trp210^{InlC}, despite the indole group of Trp210^{InlC} flipping over in one complex. A van der Waals contact between Val188^{InlC} and Val1521^{Tuba} is another invariant feature (Figure 3 a) stabilized by adjacent Ile166^{InlC}, which also stabilizes the stacking of Arg144^{InlC} and Tyr1522^{Tuba}. Only a single invariant water molecule bridges InlC and Tuba SH3-6. Located immediately adjacent to the central Asn1569^{Tuba}, it stabilizes the central Asn1569^{Tuba}/ Phe146^{InlC} stacking through hydrogen bonds to Asp148^{InlC} and Arg1572^{Tuba}.

InlC/Tuba SH3-6 complex formation

Gel filtration experiments indicate InlC/Tuba SH3-6 complex formation to be distinctly pH dependent with optimal binding at pH 7 - 7.5 but declining above pH 8. Binding assays and ITC analyses were accordingly performed in PBS pH 7.4. Molecular interactions observed in the crystal structure were corroborated qualitatively by co-purification binding assays combining wt Tuba and InlC or single-residue variants (Figure S1). InlC was stoichiometrically retained for InlC^{wt}/Tuba SH3-6^{wt} (Figure S1, lane 2), InlC^{K173A}/Tuba SH3-6^{wt} (lane 3) and InlC^{wt}/Tuba SH3-6^{P1529A} (lane 7), where modified residues lie outside the interaction surface. For substitutions within the interface significantly less InlC is retained (lanes 4 to 6), confirming the crystal structure.

Affinities of InlC/Tuba SH3-6 complexes were quantified by ITC (Figure 3 b). Freshly purified wild-type proteins show exothermic, single-site, one-step, 1:1 binding and a dissociation constant, $K_D = 5.4 \pm 0.2 \mu\text{M}$ in good agreement with $9 \mu\text{M}$ determined by surface plasmon resonance spectroscopy (Rajabian et al., 2009). InlC^{K173A}/Tuba SH3-6^{wt} has an equivalent $K_D = 5.0 \pm 0.6 \mu\text{M}$. Much weaker binding is observed for InlC^{F146A}/Tuba SH3-6^{wt}

($487 \pm 298 \mu\text{M}$) and InlC^{wt}/Tuba SH3-6^{V1521R} ($273 \pm 145 \mu\text{M}$), confirming the critical role of the modified residues. InlC^{wt}/Tuba SH3-6^{N1569R} has a nine-fold decreased K_D ($48.8 \pm 10.5 \mu\text{M}$) relative to the wt complex, similar to Tuba SH3-6/proline-rich peptides above.

Impact of the F146A mutation in InlC on cell-cell spread in cultured human cells

To address the physiological relevance of the InlC/SH3-6 crystal structure (Figures 2 and 3), we created an *Lm* strain *inlC*^{F146A} isogenic to wild-type *Lm* (WT) but whose chromosomal *inlC* gene encodes InlC^{F146A}. Comparing expression of *inlC* for *inlC*^{F146A} and WT strains in broth culture and in infected human cells indicates indistinguishable levels of InlC (Figure S2). Listerial spreading rates in cultured human cells may thus be compared. Listerial strain Δ *inlC* with deleted *inlC* was used as negative control.

Spreading efficiencies for WT, *inlC*^{F146A} and Δ *inlC* *Lm* strains were assessed in polarized human enterocyte cell line Caco-2 BBE1 by measuring the size of bacterial infection foci (Figure 4 a i). We find that *inlC*^{F146A} produces smaller foci than WT and is compromised for cell spread comparable to Δ *inlC* strain (Figure 4 a ii). For effects of *inlC*^{F146A} on protrusion formation, we quantified protrusions in confluent human cells as labeled projections from host cells expressing Enhanced Green Fluorescent Protein (EGFP) into cells lacking EGFP (Figure 4 b i). Quantification of protrusion formation by WT, Δ *inlC* and *inlC*^{F146A} strains indicate attenuated cell spread for *inlC*^{F146A} – similar to Δ *inlC* (Figure 4 b ii). *Lm* infection of Caco-2 BBE1 cells causes curving or slackening of normally linear apical junctions whereas Δ *inlC* strain does not (Rajabian et al., 2009). Despite incomplete understanding of junctional alterations, it has been linked to diminished cortical tension at the host plasma membrane and increased bacterial spread (Rajabian et al., 2009). Strain *inlC*^{F146A} does not alter the structure of host cell junctions, similar to Δ *inlC* (Figure 5). Findings in Figures 4 and 5 demonstrate a critical role for Phe146 of InlC in spreading and junctional alterations, supporting the physiological significance of the crystallographic InlC/Tuba SH3-6 complex.

Discussion

Pathogens whether viral, bacterial or eukaryotic each evolve distinct molecular strategies to undermine host processes and colonize habitats from which they are customarily excluded. A number of such virulence mechanisms have been characterized. However, to fully comprehend the complexity of the underlying processes requires information at different levels of resolution from the entire organism down to atomic details. Understanding the delicate balance of host infection through (at least initial) minimal disruption allows for the development of new counter-strategies while the molecular tools provided may be used to interrogate the intricacies of central host processes. InlC of *Listeria monocytogenes* is an excellent case in point, revealing how a relatively simple molecule may locally interfere with the host cytoskeleton to facilitate listerial cell-cell spread.

Specificity of Tuba SH3-6 peptide interactions

Src Homology 3 (SH3) domains are non-catalytic eukaryotic domains, first observed in Src related protein kinases (Mayer et al., 1988; Stahl et al., 1988) involved in signaling and cytoskeletal interactions through recognition of PXXP motifs in target proteins (Li, 2005). Tuba is a multi-domain scaffolding protein involved in cytoskeletal network assembly. Its sixth, C-terminal SH3 domain (Tuba SH3-6) specifically binds N-WASP and several other actin regulatory proteins through their proline-rich regions (Salazar et al., 2003).

The crystal structures of Tuba SH3-6/N-WASP (**PPPALPSSAPSG**) and Mena (**PPPPLPSGPAYA**) peptide complexes reveal that the poly-proline II helices bind in a class II orientation (Lim et al., 1994). Dissociation constants of 46.5 μM for Tuba SH3-6/N-WASP and 72.5 μM for /Mena indicate weak but specific protein/peptide interactions comparable to other SH3/peptide interactions (Li, 2005). The similarity of the N-WASP and Mena peptide sequences emphasize the ability of Tuba SH3-6 to interact with different target proteins depending on its localization and cellular process. The higher affinity of Tuba SH3-6 for the

N-WASP over the Mena peptide may be due to the larger hydrophobic surface provided by Pro10^{N-WASP} as compared to Ala10^{Mena}. This is particularly relevant as Pro6 and Pro10 of N-WASP sandwich the indole group of Trp1554^{Tuba} stabilizing the peptide in the binding groove.

Mode of interaction between InlC and Tuba SH36

The LRR domain of InlC and the SH3-6 domain of Tuba are both quintessential protein-protein interaction domains, each characterized by a unique binding mode to selectively interact with its partner proteins. The intricacies of each binding mode mean that they can hardly be accommodated in the same complex raising the question as to which will dominate.

Previously, an RXXK motif (residues 170-173) in InlC was proposed to act as a decoy target for Tuba SH3-6 (Rajabian et al., 2009) supported by a Lys173 to alanine substitution (Figure 2 C) which reduced InlC/Tuba SH3-6 affinity *in vitro* and impaired listerial cell spread *in vivo* (Leung et al., 2013). Unexpectedly, however, the InlC/Tuba SH3-6 crystal structure does not confirm InlC as a decoy for Tuba SH3-6. Instead, InlC clasps Tuba SH3-6 through its concave LRR domain β -sheet (Figure 2 A). Arg170 of the proposed RXXK motif does indeed directly participate in the interaction. Lys173, however, is in a loop adjacent to the LRR parallel β -sheet, 18 Å from Arg170 (Figure 2 C) and not involved in the interaction to SH3-6. Qualitative (Figure S1) and quantitative (Figure 3 B) *in vitro* binding studies of InlC variant K173A correspondingly show no difference in its affinity towards Tuba SH3-6 relative to wt InlC. Variant K173A thus unexpectedly functions as a control in that a residue not involved in the interaction in the crystal structure does not affect binding *in vitro*. By contrast, changing residues observed to be structurally involved in the interaction, in particular Phe146^{InlC}, affect not only *in vitro* recognition but induce a loss of interaction *in vivo* as well.

We hypothesize that Lys173 may be critical for the interaction of InlC with full-length Tuba in complex with its physiological partners, an aspect that our reductionist approach is currently unable to ascertain.

InlC displaces the proline-rich motif of N-WASP from Tuba allowing cell-to-cell spread

The multidomain scaffold protein Tuba is essential for cortical actin tension in cell–cell junctions whereas its depletion slackens the junctions (Otani et al., 2006). While a full molecular understanding of Tuba remains to be revealed, it is known to localize to cell–cell junctions by interacting with ZO-1, to activate the small GTPase Cdc42 through its DH-domain, and to recruit N-WASP via its C-terminal SH3 domain (Otani et al., 2006).

InlC and N-WASP compete for Tuba SH3-6 (Rajabian et al., 2009). Comparing the crystal structures of InlC/Tuba SH3-6 and N-WASP/Tuba SH3-6 indicates the affected surface area of Tuba SH3-6 to be largely distinct, overlapping in a mere five residues (grey in Figure 6 B and C) - four of which are conserved for peptide binding in SH3 domains. The overlap between the two interaction surfaces nevertheless suffices for InlC to block the peptide binding groove preventing Tuba SH3-6 binding N-WASP during listerial infection (Figure 6**Error! Reference source not found.** A).

The InlC/Tuba SH3-6 crystal structure identifies critical residues within the interface and hence for the function of InlC during cell-cell spreading. The physiological relevance of the detailed interaction is corroborated by replacing the central residue Phe146 by alanine in both heterologous InlC production and in *Lm*. *In vitro* this modification largely abrogates the InlC/Tuba SH3-6 interaction, while *in vivo* bacterial dissemination is reduced to levels seen for a $\Delta inlC$ mutant. A single point mutation thus has the same effect as the deletion of InlC, confirming Phe146 to be critical for InlC to out-compete N-WASP for Tuba SH3-6.

The affinity of InlC for Tuba SH3-6 is eight-fold higher than that of Tuba SH3-6 for the N-WASP poly-proline motif – though the relative abundance of individual proteins is also

critical in determining the final equilibrium. During a listerial infection, moderate local InIC concentrations could rapidly displace N-WASP relaxing the cortical tension of apical junctions allowing bacterial cell-to-cell spread (Rajabian et al., 2009).

Implications of InIC/Tuba SH3-6 interactions for small animal studies

Despite highly conserved sequences for the targets of both listerial virulence factors InIA and InIB, natural variations of critical residues in non-human species have been shown to interfere with their respective functions. InIA thus does not bind murine E-cadherin *inter alia* due to the exchange of Pro16 of human E-cadherin by glutamate (Lecuit et al., 1999; Schubert et al., 2002; Wollert et al., 2007). InIB similarly does not bind the Met receptor of rabbit and guinea pig (Khelef et al., 2006). Minor modifications in target proteins may hence result in species barriers – limiting the suitability of small animal models in studying molecular mechanisms underlying an infection. Amino acids critical for Tuba SH3-6 recognition are mostly conserved in model organisms such as mouse, guinea pig and rabbit. In guinea pig, all residues are conserved, while Val1521 of human Tuba is replaced by slightly larger isoleucine in mice potentially increasing affinity (Figure 6 C). In rabbits, critical Asn1569^{Tuba} is replaced by smaller serine almost certainly weakening the interaction. Significant differences in the effectiveness of cell-to-cell spread in different mammals may thus result.

Tuba SH3-6 oligomerization

SH3 domains are often assumed to be monomeric despite SH3 oligomerization having been shown to affect function in Esp8 (Kishan et al., 1997) and tyrosine kinase Csk (Levinson et al., 2009), or through additional oligomerization domains (Derivery and Gautreau, 2010). Arp2/3 complex activation thus appears to depend on N-WASP recruitment following SH3-domain oligomerization (Derivery and Gautreau, 2010; Kessels and Qualmann, 2006; Padrick et al., 2008). The virulence factor EspF_U of enterohemorrhagic *E. coli*, by contrast, uses tandem proline-rich repeats to cluster ‘insulin receptor tyrosine kinase substrate’ (IRTKS) to

reprogram the actin polymerization machinery (Aitio et al., 2010; Cheng et al., 2008; Sallee et al., 2008). EspF_U and InIC follow diametrically opposite strategies in targeting eukaryotic SH3-domains: Whereas EspF_U accumulates N-WASP/IRTKS to potentiate actin polymerization, InIC interrupts Tuba/N-WASP interaction to eliminate cortical actin tension.

Tuba SH3-6 oligomerizes both with and without peptide ligands, forming monomers, dimers and tetramers according to gel filtration (Figure S5). Tuba may thus also be regulated by SH3-6 domain oligomerization. Three crystal packing arrangements for two Tuba SH3-6/peptide complexes (Table 1) fortuitously all contain identical asymmetric Tuba SH3-6 dimers (Figure S4 b), which we postulate correspond to *in vitro* SH3-6 dimers. The asymmetric dimers create helical filaments extending through the crystal (Figure S4 a). The physiological relevance of Tuba oligomerization and its impact during listerial infection, however, remains unclear.

Internalin family interactions

Crystal structures of the two other members of the internalin family of listerial virulence factors, InIA and InIB, respectively complexed to their physiological targets E-cadherin and the Met receptor have previously been reported (Niemann et al., 2007; Schubert et al., 2002). In InIA, the 15-stranded parallel β -sheet of the LRR binds the N-terminal Ig-like domain of human E-cadherin (hEC1) (Schubert et al., 2002). The dominant interface of InIB/Met receptor also involves the parallel β -sheet of the InIB LRR contacting the Ig1 domain of Met (Niemann et al., 2007), augmented by contacts between the InIB LRR and the Met PSI domain, the InIB Ig-like interrepeat domain and the Met Sema domain, as well as InIB/InIB contacts for Met receptor dimerization (Ferraris et al., 2010).. These crystal structures define a “classical” mode of interaction for the internalin protein family in which the parallel β -sheet of the curved LRR and in particular aromatic amino acids dominate the interaction (Machner et al., 2003). The crystal structure of InIC/Tuba SH3-6 indicates that InIC also broadly follows this trend.

Interestingly, InlA, InlB and InlC all bind small, predominantly β -strand domains of human proteins: hEC1 of E-cadherin, Ig1 of the Met receptor and the SH3-6 domain of Tuba, respectively. The interaction details are, nevertheless unique to each case with InlA predominantly interacting with β -strand residues of hEC1, InlB binding loop residues of Met Ig1, and InlC recognizing β -strand, loop and 3_{10} -helix residues of Tuba SH3-6. Potentially, the preference of internalin-family proteins for small β -sheet domains of human proteins is dictated by the curvature of the LRR β -sheet rather than any particular type of interaction. Extended to the interaction of InlC with its second target protein IKK α (Gouin et al., 2010), would identify its β -strand-rich kinase or ubiquitin-like domain as potential targets.

Conclusions

Cell-cell spread is a central feature of virulence in *Listeria monocytogenes*. Cortical actin tension of polarized cells physically limits remodeling of the cell membrane, protrusion formation and hence cell-cell spread. Cortical tension *inter alia* depends on human Tuba, through its SH3-6 domain, specifically interacting with a proline rich peptide of N-WASP. InlC undermines cortical tension by severing this interaction – not, however, by exploiting the peptide recognition of Tuba SH3-6. Instead the InlC LRR domain actively binds Tuba SH3-6 to block the SH3 binding groove and displace N-WASP through its higher affinity. Given the abundance of SH3 domains and their central role in signaling it is likely that the strategy of InlC in interfering with SH3 domain function is used by other microbial pathogens.

Experimental Procedures

Cloning and protein production

DNA coding for Tuba SH3-6 (residues 1513-1577) was inserted into pGEX-6P-1 (GE Healthcare) for GST-fusion protein. pET21a plasmid for InlC is described in (Rajabian et al.,

2009). Variant plasmids were prepared by QuikChange mutagenesis. For primers see Table S1. InlC-His₆ and variants were produced in *E. coli* BL21 (DE3) (Invitrogen) in lysogeny broth (LB) medium, 0.1 mg/mL ampicillin (amp), 37°C. Induction at OD_{600nm} ~0.7 was by 50 µM IPTG, 20°C, 15 h. Cells were centrifuged (15 min, 6000 g, 4°C) and sonicated in 25 mM Tris pH 8, 300 mM NaCl and 10 mM imidazole. InlC-His₆ from centrifugation (45 min, 37 000 g, 4°C) supernatant was purified by Ni-NTA affinity chromatography (Sepharose Superflow resin, Qiagen) eluting with 10-500 mM imidazole gradient in 25 mM Tris pH 8, 100 mM NaCl, and anion exchange chromatography (MonoQ HR10/10, GE Healthcare) in 10 mM Tris pH 8, 10-500 mM NaCl gradient. GST-Tuba SH3-6 production: *E. coli* BL21-CodonPlus (Stratagene), LB medium, 34 µg/ml chloramphenicol, 100 µg/mL amp. Expression: 100 µM IPTG, overnight, 20°C. Purification: affinity chromatography on glutathione agarose (GA) 4B beads (Macherey-Nagel), protein cleavage by 3C protease, 25°C, 15 h, and gel filtration (Superdex 75 10/30, GE Healthcare) in 10 mM Tris pH 7, 10 mM NaCl. Sample purity was assessed by SDS PAGE. Final protein concentration was 30 mg/ml, stored at 4°C or -20°C.

Crystallization and structure determination

Chemically synthesized peptides (Werner Tegge, Helmholtz-Centre for Infection Research, Germany) of human N-WASP (residues 346-357) and murine Mena (547-558) were dissolved in ddH₂O, mixed 3:1 with Tuba SH3-6 and incubated: 4°C, 1 h. Crystallization was in 24-well hanging drop vapor-diffusion plates with 1 µL reservoir, 1 µL protein (28 mg/mL) and 0.1 µL of crushed crystals. Crystals of Tuba SH3-6/Mena peptide grew in 2-3.3 M NaCl, 0.1 M Bis-Tris pH 5.5, 1 day, 16°C, those of Tuba SH3-6/N-WASP peptide in 4-10 days, 16°C under the same conditions. 30% glycerol (v/v) in reservoir solution was used for cryo protection. Lead conditions for InlC/Tuba SH3-6 were identified using commercial screens (Qiagen). Variant InlC^{Y246A-Y247A} mixed 1:1.5 with Tuba SH3-6, total protein concentration 20 mg/ml, was incubated: 4°C, 1 h. 300 nL protein, 300 nL reservoir solution and 50 nL lysozyme crystal

nuclei were pipetted into low-profile 96-well plates (Greiner Bio One). Crystals grew after 3 months at 16°C in 1.6 M NaKHPO₄, 0.1 M HEPES pH 7.5, supplemented by 30% (v/v) glycerol for cryoprotection.

Initial data for Tuba SH3-6/peptide complexes were collected in-house on a Rigaku HighFlux Home Lab system using HKL3000 (Minor *et al.*, 2006) for data processing. The structure was solved by molecular replacement using Phaser (McCoy *et al.*, 2005) with PDB 1ZUU as search model pruned by Chainsaw (Schwarzenbacher *et al.*, 2004). Refmac5 structure refinement (Murshudov *et al.*, 1997) was alternated with manual rebuilding in Coot (Emsley and Cowtan, 2004). Local NCS and TLS refinement improved the R_{free} slightly and were therefore used where appropriate. Final data sets were collected at beamline PROXIMA1, SOLEIL, Paris on a Pilatus detector. Data was processed with XDS (Kabsch, 2010). Data and refinement statistics are listed in Table 1.

X-ray diffraction data for InlC/Tuba SH3-6 were collected in-house and processed as above. The structure was solved by molecular replacement using Phaser (McCoy *et al.*, 2005) with InlC (PDB 1XEU) and the refined Tuba SH3-6 structure as search models. Refinement and model building were as above.

Figures were prepared with PyMOL (www.pymol.org). Buried surface areas were calculated and Search model for Tuba SH3-6/peptide was PDB 1ZUU, for InlC/Tuba SH3-6 PDB 1XEU and refined Tuba SH3-6. Refinement used Refmac5 (Murshudov *et al.*, 1997) alternated with Coot (Emsley and Cowtan, 2004). See Table 1. Figures were prepared with PyMOL (www.pymol.org). Surfaces were analyzed with PISA (Krissinel and Henrick, 2007).

Binding studies

Protein-protein and -peptide interactions were analyzed in PBS at 25°C using an iTC₂₀₀ microcalorimeter (MicroCal, USA). For Tuba SH3-6/N-WASP (Mena), 18 2- μ l aliquots of 1.5 mM (3 mM) peptide were added to 150 μ M Tuba SH3-6. Experiments were repeated

twice. For InlC/Tuba SH3-6 interactions, 25 1.5- μ l aliquots of 0.80 mM InlC were injected into 200 μ l of 80 μ M Tuba SH3-6. Data were processed, corrected for heat of dilution and analyzed using “one set of sites” mode of Origin v7.0 with MicroCal ITC add-on software. GST-Tuba SH3-6 or variants were eluted from glutathione agarose 4B (GA) beads (Macherey-Nagel) by 20 mM reduced glutathione in PBS pH 7.4 and purified by gel filtration (Superdex 75 10/30, GE Healthcare). 300 μ g GST-Tuba SH3-6, 300 μ g InlC, and 25 μ L GA beads in 1 mL PBS pH 7.4 were incubated 20 min, 4°C. Controls for unspecific interactions were 200 μ g GST/300 μ g InlC and 300 μ g InlC plus 25 μ L GA each. The GA beads were washed thrice with 1 mL PBS to remove unbound proteins. Beads were suspended in 200 μ L PBS and InlC/Tuba SH3-6 released proteolytically by 1 μ g 3C protease at 23°C, 15 h. 10 μ L of the eluant was analyzed by SDS-PAGE.

Bacterial strains and mammalian cell lines

Lm strains wild-type EGD (WT), *inlC* deletion (Δ *inlC*) (Engelbrecht., 1996; Rajabian et al., 2009) and *inlC*^{F146A} mutant, constructed by allelic replacement, are isogenic. Codon 146 of *inlC*^{F146A} was changed from phenylalanine to alanine by QuikChange kit (Agilent) in pUC18. For primers see Table S1. The mutant allele was subcloned into pLSV101. Homologous insertion into the *Lm* chromosome was as described (Wuenschel et al., 1991). Clones with F146A mutation were identified by PCR and confirmed by sequencing. Bacterial strains were grown in Brain Heart Infusion (BHI) agar or broth. The human enterocyte cell line Caco-2 BBE1 (ATTC CRL-2102) was grown in 6-well plates on transwell permeable supports (Costar 0.4 μ M) as in (Rajabian et al., 2009). Cells were grown for 4 days prior to infection for InlC expression and protrusion studies, and 7 days for cell spread and apical junction analysis experiments.

Analysis of InlC^{F146A} expression by Lm

For *inlC* quantification in BHI broth, equal supernatant volumes (6000 rpm, 3 min) from 15 h cultures of WT, $\Delta inlC$ or *inlC^{F146A}* strains were loaded onto 10% SDS/polyacrylamide gels, transferred to PVDF membranes and Western blotted with polyclonal anti-InlC antibodies. Detection was with ECL Plus (GE Healthcare) and a Molecular Imager Chemidoc XRS Chemidoc system (Biorad). For analysis of InlC expression in infected human cells, Caco-2 BBE1 cells were uninfected or infected with WT, $\Delta inlC$, or *inlC^{F146A}* for 1.5 h without and 4.0 h with 20 $\mu\text{g/ml}$ gentamicin to eliminate extracellular bacteria. Infected cells were washed in PBS and resuspended in lysis buffer: 25 mM Tris-HCl pH 7.5, 150 mM NaCl, 1% Triton X-100, 1 mM PMSF, 10 $\mu\text{g/ml}$ aprotinin and leupeptin. A lysate fraction was used to determine bacterial colony forming units (CFUs), the remainders stored at $-80\text{ }^{\circ}\text{C}$. Viable intracellular WT, $\Delta inlC$, and *inlC^{F146A}* bacteria were calculated. Cell lysate volumes with equal numbers of intracellular bacteria were used for immunoprecipitation with InlC antibodies or rabbit IgG as control (Shen et al., 2000), using 10 μl anti-InlC antibodies.

Assessment of cell-cell spread

Caco-2 BBE1 cells were infected with WT, $\Delta inlC$, or *inlC^{F146A}* strains for 1.5 h without and 10.5 h with gentamicin. PBS washed cells were fixed in 3% paraformaldehyde. Samples were permeabilized, antibody labeled and mounted (Sun et al., 2005). Intra- and extracellular bacteria were differentially labeled by rabbit anti-*Lm* antibody (Becton Dickenson, 223021) before and after human cell permeabilization (Sun et al., 2005). Secondary antibodies were anti-rabbit coupled to AlexaFluor488 or 647 (Life Technologies). Extracellular bacteria are thus both AlexaFluor488 and 647 labeled, intracellular bacteria only with AlexaFluor488. Phalloidin conjugated AlexaFluor555 was used for filamentous actin in human cells. Spreading efficiencies of WT, $\Delta inlC$, or *inlC^{F146A}* strains were determined from focal surface areas with intracellular bacteria (Zeiss LSM 510 confocal microscope) with cell borders detected by F-actin labeling. Regions around foci with contiguous infected human cells were

delimited and surface areas measured by Image J software (version 1.43r, <http://rsbweb.nih.gov/ij>). 25 foci were measured for each strain in each experiment. Surface areas were normalized using WT strain values.

Quantification of bacterial protrusion formation

Protrusion efficiency was quantified by counting protrusions from EGFP expressing human Caco-2 BBE1 cells into EGFP-negative cells (Rajabian et al., 2009). 3 days after transfection, cells were infected with WT, $\Delta inlC$, or $inlC^{F146A}$ strains for 1.5 h without and 4 h with gentamicin. Cells were washed in PBS, fixed, permeabilized, and labeled with anti-*Lm* antibodies and phalloidin-AlexaFluor555 to detect F-actin. Images of 1 μ m sections were taken on a Zeiss LSM 710 confocal microscope with diode (405 nm), multiline argon (458/488/514), helium-neon 1 (543) and 2 (633) lasers. Protrusions, F-actin comet tails in the cell body, and bacteria decorated with symmetric F-actin in the cell body of each EGFP-positive cell were quantified. 50 protrusions were scored for each strain and experiment. Protrusion efficiency is the percentage of bacteria in protrusions relative to total F-actin associated bacteria. Efficiencies were normalized to the wild-type strain.

Analysis of cell junction structure

Caco-2 BBE1 cells were uninfected or infected with WT, $\Delta inlC$, or $inlC^{F146A}$ strains for 1.5 h without and 4 h with gentamicin. Cells were fixed and labeled with rabbit anti-*Lm* antibodies, mouse anti-ZO1 antibodies and phalloidin-AlexaFluor555. ZO1 labeling marks apical junctions. Images of 1 μ m sections were taken on a Zeiss LSM confocal microscope. Only infected cells with F-actin decorated intracellular bacteria were analyzed. Cell junction morphology was assessed from junction linearity (Otani et al., 2006; Rajabian et al., 2009) using 'linear index' values: 1, perfect linearity, >1, increasing curvature. 100 junctions were assessed for each condition and experiment.

Acknowledgements

We gratefully acknowledge beam time at PROXIMA1, SOLEIL, Paris, France. We thank Pierre Legrand and Andrew Thompson for help with data collection, Dave Woolley for support with ITC experiments, Werner Tegge for peptide synthesis, and Martin Heisig for advice on *Lm* strain construction. We acknowledge financial support by the Medical Research Council and the National Research Foundation of South Africa to Wolf-Dieter Schubert, and by the National Institutes of Health (grant R01AI085072) to Keith Ireton.

References

- Aitio,O., Hellman,M., Kazlauskas,A., Vingadassalom,D.F., Leong,J.M., Saksela,K., and Pemi,P. (2010). Recognition of tandem PxxP motifs as a unique Src homology 3-binding mode triggers pathogen-driven actin assembly. *Proc. Natl. Acad. Sci. U. S. A* *107*, 21743-21748.
- Alexandropoulos,K., Cheng,G., and Baltimore,D. (1995). Proline-rich sequences that bind to Src homology 3 domains with individual specificities. *Proc. Natl. Acad. Sci. U. S. A* *92*, 3110-3114.
- Cheng,H.C., Skehan,B.M., Campellone,K.G., Leong,J.M., and Rosen,M.K. (2008). Structural mechanism of WASP activation by the enterohaemorrhagic *E. coli* effector EspF(U). *Nature* *454*, 1009-1013.
- Cossart,P. (2007). *Listeriology (1926-2007): the rise of a model pathogen*. *Microbes. Infect.* *9*, 1143-1146.
- Derivery,E. and Gautreau,A. (2010). Generation of branched actin networks: assembly and regulation of the N-WASP and WAVE molecular machines. *Bioessays* *32*, 119-131.
- Emsley,P. and Cowtan,K. (2004). Coot: model-building tools for molecular graphics. *Acta Crystallogr. D. Biol. Crystallogr.* *60*, 2126-2132.
- Engelbrecht.,F. (1996). A new PrfA-regulated gene of *Listeria monocytogenes* encoding a small, secreted protein which belongs to the family of internalins. *Mol. Microbiol.* *21*, 823-837.

- Ferraris,D.M., Gherardi,E., Di,Y., Heinz,D.W., and Niemann,H.H. (2010). Ligand-mediated dimerization of the Met receptor tyrosine kinase by the bacterial invasion protein InlB. *J. Mol. Biol.* *395*, 522-532.
- Gouin,E., Adib-Conquy,M., Balestrino,D., Nahori,M.A., Villiers,V., Colland,F., Dramsi,S., Dussurget,O., and Cossart,P. (2010). The *Listeria monocytogenes* InlC protein interferes with innate immune responses by targeting the I{kappa}B kinase subunit IKK{alpha}. *Proc. Natl. Acad. Sci. U. S. A* *107*, 17333-17338.
- Hamon,M., Bierne,H., and Cossart,P. (2006). *Listeria monocytogenes*: a multifaceted model. *Nat. Rev. Microbiol.* *4*, 423-434.
- Kabsch,W. (2010). XDS. *Acta Crystallogr. D. Biol. Crystallogr.* *66*, 125-132.
- Kessels,M.M. and Qualmann,B. (2006). Syndapin oligomers interconnect the machineries for endocytic vesicle formation and actin polymerization. *J. Biol. Chem.* *281*, 13285-13299.
- Khelef,N., Lecuit,M., Bierne,H., and Cossart,P. (2006). Species specificity of the *Listeria monocytogenes* InlB protein. *Cell Microbiol.* *8*, 457-470.
- Kishan,K.V., Scita,G., Wong,W.T., Di Fiore,P.P., and Newcomer,M.E. (1997). The SH3 domain of Eps8 exists as a novel intertwined dimer. *Nat. Struct. Biol.* *4*, 739-743.
- Krissinel,E. and Henrick,K. (2007). Inference of macromolecular assemblies from crystalline state. *J. Mol. Biol.* *372*, 774-797.

- Larson,S.M. and Davidson,A.R. (2000). The identification of conserved interactions within the SH3 domain by alignment of sequences and structures. *Protein Sci.* 9, 2170-2180.
- Lecuit,M., Dramsi,S., Gottardi,C., Fedor-Chaiken,M., Gumbiner,B., and Cossart,P. (1999). A single amino acid in E-cadherin responsible for host specificity towards the human pathogen *Listeria monocytogenes*. *EMBO J.* 18, 3956-3963.
- Leung,N., Gianfelice,A., Gray-Owen,S.D., and Ireton,K. (2013). Impact of the *Listeria monocytogenes* protein InlC on infection in mice. *Infect. Immun.* 81, 1334-1340.
- Levinson,N.M., Visperas,P.R., and Kuriyan,J. (2009). The tyrosine kinase Csk dimerizes through Its SH3 domain. *PLoS. One.* 4, e7683.
- Li,S.S. (2005). Specificity and versatility of SH3 and other proline-recognition domains: structural basis and implications for cellular signal transduction. *Biochem. J.* 390, 641-653.
- Lim,W.A., Richards,F.M., and Fox,R.O. (1994). Structural determinants of peptide-binding orientation and of sequence specificity in SH3 domains. *Nature* 372, 375-379.
- Machner,M.P., Frese,S., Schubert,W.D., Orian-Rousseau,V., Gherardi,E., Wehland,J., Niemann,H.H., and Heinz,D.W. (2003). Aromatic amino acids at the surface of InlB are essential for host cell invasion by *Listeria monocytogenes*. *Mol. Microbiol.* 48, 1525-1536.
- Mayer,B.J., Hamaguchi,M., and Hanafusa,H. (1988). A novel viral oncogene with structural similarity to phospholipase C. *Nature* 332, 272-275.

- McCoy,A.J., Grosse-Kunstleve,R.W., Storoni,L.C., and Read,R.J. (2005). Likelihood-enhanced fast translation functions. *Acta Crystallogr. D. Biol. Crystallogr.* *61*, 458-464.
- Minor,W., Cymborowski,M., Otwinowski,Z., and Chruszcz,M. (2006). HKL-3000: the integration of data reduction and structure solution--from diffraction images to an initial model in minutes. *Acta Crystallogr. D. Biol. Crystallogr.* *62*, 859-866.
- Murshudov,G.N., Vagin,A.A., and Dodson,E.J. (1997). Refinement of macromolecular structures by the maximum-likelihood method. *Acta Crystallogr. D. Biol. Crystallogr.* *53*, 240-255.
- Niemann,H.H., Jager,V., Butler,P.J., van den Heuvel,J., Schmidt,S., Ferraris,D., Gherardi,E., and Heinz,D.W. (2007). Structure of the human receptor tyrosine kinase met in complex with the *Listeria* invasion protein InlB. *Cell* *130*, 235-246.
- Ooi,A., Hussain,S., Seyedarabi,A., and Pickersgill,R.W. (2006). Structure of internalin C from *Listeria monocytogenes*. *Acta Crystallogr. D. Biol. Crystallogr.* *62*, 1287-1293.
- Otani,T., Ichii,T., Aono,S., and Takeichi,M. (2006). Cdc42 GEF Tuba regulates the junctional configuration of simple epithelial cells. *J. Cell Biol.* *175*, 135-146.
- Padrick,S.B., Cheng,H.C., Ismail,A.M., Panchal,S.C., Doolittle,L.K., Kim,S., Skehan,B.M., Umetani,J., Brautigam,C.A., Leong,J.M., and Rosen,M.K. (2008). Hierarchical regulation of WASP/WAVE proteins. *Mol. Cell* *32*, 426-438.

Pons,C., Solernou,A., Perez-Cano,L., Grosdidier,S., and Fernandez-Recio,J. (2010). Optimization of pyDock for the new CAPRI challenges: Docking of homology-based models, domain-domain assembly and protein-RNA binding. *Proteins* 78, 3182-3188.

Rajabian,T., Gavicherla,B., Heisig,M., Muller-Altrock,S., Goebel,W., Gray-Owen,S.D., and Ireton,K. (2009). The bacterial virulence factor InlC perturbs apical cell junctions and promotes cell-to-cell spread of *Listeria*. *Nat. Cell Biol.* 11, 1212-1218.

Salazar,M.A., Kwiatkowski,A.V., Pellegrini,L., Cestra,G., Butler,M.H., Rossman,K.L., Serna,D.M., Sondek,J., Gertler,F.B., and De,C.P. (2003). Tuba, a novel protein containing bin/amphiphysin/Rvs and Dbl homology domains, links dynamin to regulation of the actin cytoskeleton. *J. Biol. Chem.* 278, 49031-49043.

Sallee,N.A., Rivera,G.M., Dueber,J.E., Vasilescu,D., Mullins,R.D., Mayer,B.J., and Lim,W.A. (2008). The pathogen protein EspF(U) hijacks actin polymerization using mimicry and multivalency. *Nature* 454, 1005-1008.

Schlech,W.F., III (2000). Foodborne listeriosis. *Clin. Infect. Dis.* 31, 770-775.

Schubert,W.D., Gobel,G., Diepholz,M., Darji,A., Kloer,D., Hain,T., Chakraborty,T., Wehland,J., Domann,E., and Heinz,D.W. (2001). Internalins from the human pathogen *Listeria monocytogenes* combine three distinct folds into a contiguous internalin domain. *J. Mol. Biol.* 312, 783-794.

Schubert,W.D., Urbanke,C., Ziehm,T., Beier,V., Machner,M.P., Domann,E., Wehland,J., Chakraborty,T., and Heinz,D.W. (2002). Structure of internalin, a major invasion protein of *Listeria monocytogenes*, in complex with its human receptor E-cadherin. *Cell* 111, 825-836.

Schwarzenbacher,R., Godzik,A., Grzechnik,S.K., and Jaroszewski,L. (2004). The importance of alignment accuracy for molecular replacement. *Acta Crystallogr. D. Biol. Crystallogr.* *60*, 1229-1236.

Shen,Y., Naujokas,M., Park,M., and Ireton,K. (2000). InIB-dependent internalization of *Listeria* is mediated by the Met receptor tyrosine kinase. *Cell* *103*, 501-510.

Sparks,A.B., Rider,J.E., Hoffman,N.G., Fowlkes,D.M., Quillam,L.A., and Kay,B.K. (1996). Distinct ligand preferences of Src homology 3 domains from Src, Yes, Abl, Cortactin, p53bp2, PLCgamma, Crk, and Grb2. *Proc. Natl. Acad. Sci. U. S. A* *93*, 1540-1544.

Stahl,M.L., Ferez,C.R., Kelleher,K.L., Kriz,R.W., and Knopf,J.L. (1988). Sequence similarity of phospholipase C with the non-catalytic region of src. *Nature* *332*, 269-272.

Sun,H., Shen,Y., Dokainish,H., Holgado-Madruga,M., Wong,A., and Ireton,K. (2005). Host adaptor proteins Gab1 and CrkII promote InIB-dependent entry of *Listeria monocytogenes*. *Cell Microbiol.* *7*, 443-457.

Vazquez-Boland,J.A., Kuhn,M., Berche,P., Chakraborty,T., Dominguez-Bernal,G., Goebel,W., Gonzalez-Zorn,B., Wehland,J., and Kreft,J. (2001). *Listeria* pathogenesis and molecular virulence determinants. *Clin. Microbiol. Rev.* *14*, 584-640.

Welch,M.D., Iwamatsu,A., and Mitchison,T.J. (1997). Actin polymerization is induced by Arp2/3 protein complex at the surface of *Listeria monocytogenes*. *Nature* *385*, 265-269.

Wollert,T., Heinz,D.W., and Schubert,W.D. (2007). Thermodynamically reengineering the listerial invasion complex InlA/E-cadherin. *Proc. Natl. Acad. Sci. U. S. A* *104*, 13960-13965.

Wuenscher, M.D., Kohler, S., Goebel, W., and Chakraborty, T. (1991). Gene disruption by plasmid integration in *Listeria monocytogenes*: insertional inactivation of the listeriolysin determinant *lisA*. *Mol. Gen. Genet.* 228, 177-182.

Figure Legends

Figure 1: Proline-rich peptide recognition by Tuba SH3-6. (a) Surface presentation of the Tuba SH3-6 domain. N-WASP (red) and Mena (yellow) peptides adopt equivalent conformations. (b) Conserved peptide binding SH3 residues in Tuba SH3-6 (Larson and Davidson, 2000) are colored blue, less conserved peptide binding groove residues in grey, and N-WASP peptide in red. (c) Isothermal titration calorimetry (ITC) analysis of Tuba SH3-6/N-WASP peptide: Titration heat release (upper panel) and corrected heat data are plotted against N-WASP peptide molar ratios (lower panel).

Figure 2: InlC recognition of Tuba SH3-6. (a) Translucent surfaces reveal the secondary structure of both proteins. (b) Superimposing three crystallographically independent complexes show InlC and the SH3 domain core as mostly rigid. The N- and C-termini (dotted ellipse) and most loops of Tuba SH3-6 are more variable. (c) Surfaces of InlC and of Tuba SH3-6 colored as in a. Surface areas in complex formation adopt the color of the binding partner. Magenta: Lys173^{InlC}.

Figure 3: Details of InlC/Tuba SH3-6 interaction. (a) Residues of InlC and Tuba SH3-6 involved in the intermolecular interaction in three independent complexes are shown. Aromatic residues are underlined. Hydrogen bonds are indicated by thin black dotted lines, van der Waals interactions by thick red dashed lines. (b) ITC analysis of wt Tuba SH3-6 or variants binding InlC^{wt} or variants showing corrected heat versus molar ratio.

Figure 4: Mutation of F146A in InlC attenuates cell-cell spread of *Lm*. (a) Caco-2 BBE1 cells were infected with WT, $\Delta inlC$, or $inlC^{F146A}$ strains 12 h prior to fixation and labeling: intracellular (red) and extracellular bacteria (yellow), or F-actin (blue). (i) Infection foci surface areas were measured by Image J (<http://rsbweb.nih.gov/ij>). (ii) Bacterial spreading was quantified using mean relative focal surface areas for WT, $\Delta inlC$, or $inlC^{F146A}$ infections from three experiments. ANOVA analysis: $P < 0.0001$. *, $P < 0.05$ relative to WT control. Scale bars - 20 μm . (b) Effect of F146A on bacterial protrusion formation. (i) EGFP expressing Caco-2 BBE1 cells were infected with *Lm* for 5.5 h, fixed and labeled for confocal microscopy. Protrusions (*) were identified as EGFP-positive F-actin tails projecting from transfected cells into EGFP-negative cells. Bacteria with F-actin tails (arrow) and symmetric F-actin (arrowhead) within EGFP-positive cells were also scored. Protrusion formation efficiency is the percentage of total F-actin associated bacteria in protrusions. Scale bar - 5 μm . (ii) Relative protrusion efficiencies by WT, $\Delta inlC$, or $inlC^{F146A}$ *Lm* strain are absolute percentages normalized to WT from three experiments. Statistical analysis as for a.

Figure 5: *Lm* mutant $inlC^{F146A}$ is unable to alter apical junction morphology. (a) Apical junctions of infected Caco-2 BBE1 human cells in transwells uninfected or infected for 5.5 h with WT, $\Delta inlC$, or $inlC^{F146A}$ strains. Fixed cells were labeled for bacteria (blue), F-actin (red), and tight junction protein ZO1 (green). Asterisks indicate cells with intracellular F-actin decorated bacteria. Junctions (ZO1 labeling) in WT *Lm* infected cells are curved, those in $\Delta inlC$ or $inlC^{F146A}$ infected cells are more linear. Scale bars - 10 μm . (b) Quantification of cell junction linearity. Linear indices of junctions were determined as mean values from three experiments. Statistical analysis by ANOVA indicated $P = 0.0070$. *, $P < 0.05$ relative to the uninfected (U) control.

Figure 6: Tuba SH3-6 binding surfaces. (a) Tuba SH3-6 complexes with InlC and N-WASP peptide are overlaid. N-terminal residues of N-WASP peptide sterically clash with InlC. (b)

Residues of Tuba SH3-6 in contact with InlC or N-WASP only are in blue and pink, those in contact with both in grey. (c) Tuba SH3-6 sequence alignment for small animal hosts. Underlaid colors are as in b. Secondary structure shown in green. Residues different to human Tuba are in bold and color: yellow – not in interface, red – affecting binding.

Table 1: Crystallographic data and refinement statistics

	InlC [¶] / Tuba SH3-6	Tuba SH3-6/ N-WASP peptide	Tuba SH3-6/ N-WASP peptide	Tuba SH3-6/ Mena peptide
PDB codes	4cc4	4cc2	4cc7	4cc3
Diffraction data				
Wavelength (Å)	1.54	0.98	0.98	0.98
Space group	<i>P2₁2₁2₁</i>	<i>P2₁2₁2₁</i>	<i>P4₁</i>	<i>H3</i>
Unit cell axes a/b/c (Å)	89.7/101.7/126.9	48.8/70.3/38.0	88.5/88.5/69.7	115.9/115.9/73.1
Molecules/AU	3+3	2+2	7+7	4+4
Resolution range* (Å)	15-2.6 (2.64-2.60)	50-1.55 (1.64-1.55)	50-1.97 (2.09-1.97)	50-1.97 (2.09-1.97)
Unique reflections*	36275 (1809)	18418 (2994)	38387 (6115)	25648 (3967)
Completeness (%)*	100 (100)	93.4 (95.8)	99.8 (99.2)	99.0 (95.5)
Redundancy*	5.5 (5.5)	2.8 (2.7)	6.0 (6.0)	4.2 (4.1)
I/σ _I *	21.4 (3.0)	15.5 (2.7)	20.7 (2.6)	16.9 (3.0)
R _{merge} (%)*	10.2 (66.1)	4.2 (38.6)	5.2 (70.8)	4.3 (42.4)
Refinement statistics				
R _{work} / R _{free} (%)	19.9/26.1	17.0/21.8	17.8/21.5	18.1/21.5
Refined atoms: protein/ligand/solvent	8069/75/280	1238/44/147	4154/43/251	2405/10/149
Multiple conformation side chains	36	19	37	11
Root mean square deviation from ideal				
Bond lengths (Å)	0.014	0.023	0.019	0.019
Bond angles (°)	1.75	2.36	1.96	2.05
Ramachandran plot				
Preferred/allowed/ outliers (%)	92.9/6.0/1.1	99.2/0.8/0	97.6/2.4/0	96.3/3.7/0

* Numbers in parentheses indicate values corresponding to the shell of highest resolution

[¶] Note that Tuba SH3-6 was co-crystallized with InlC-variant Y246A-Y247A

Figure 1
[Click here to download high resolution image](#)

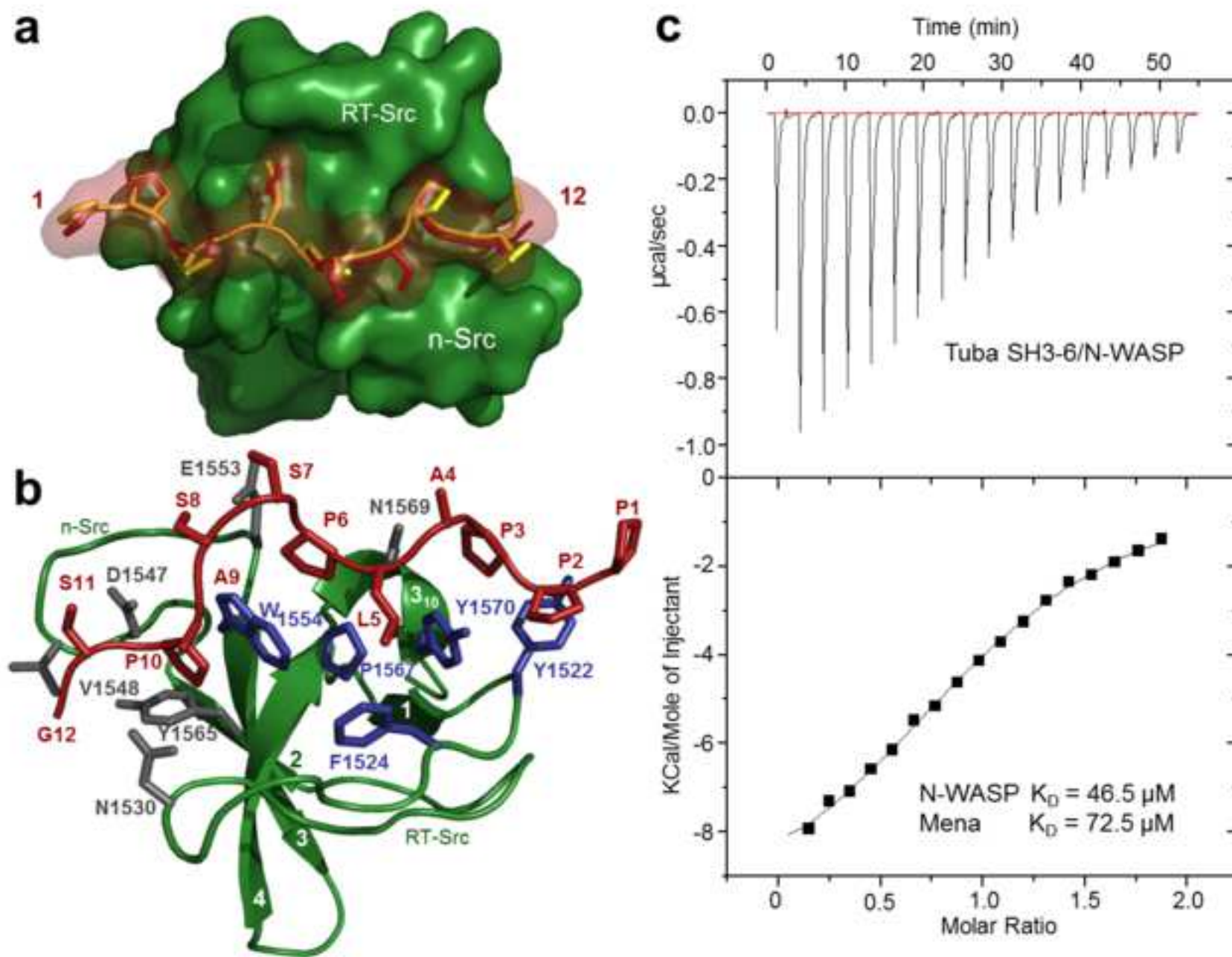


Figure 2
[Click here to download high resolution image](#)

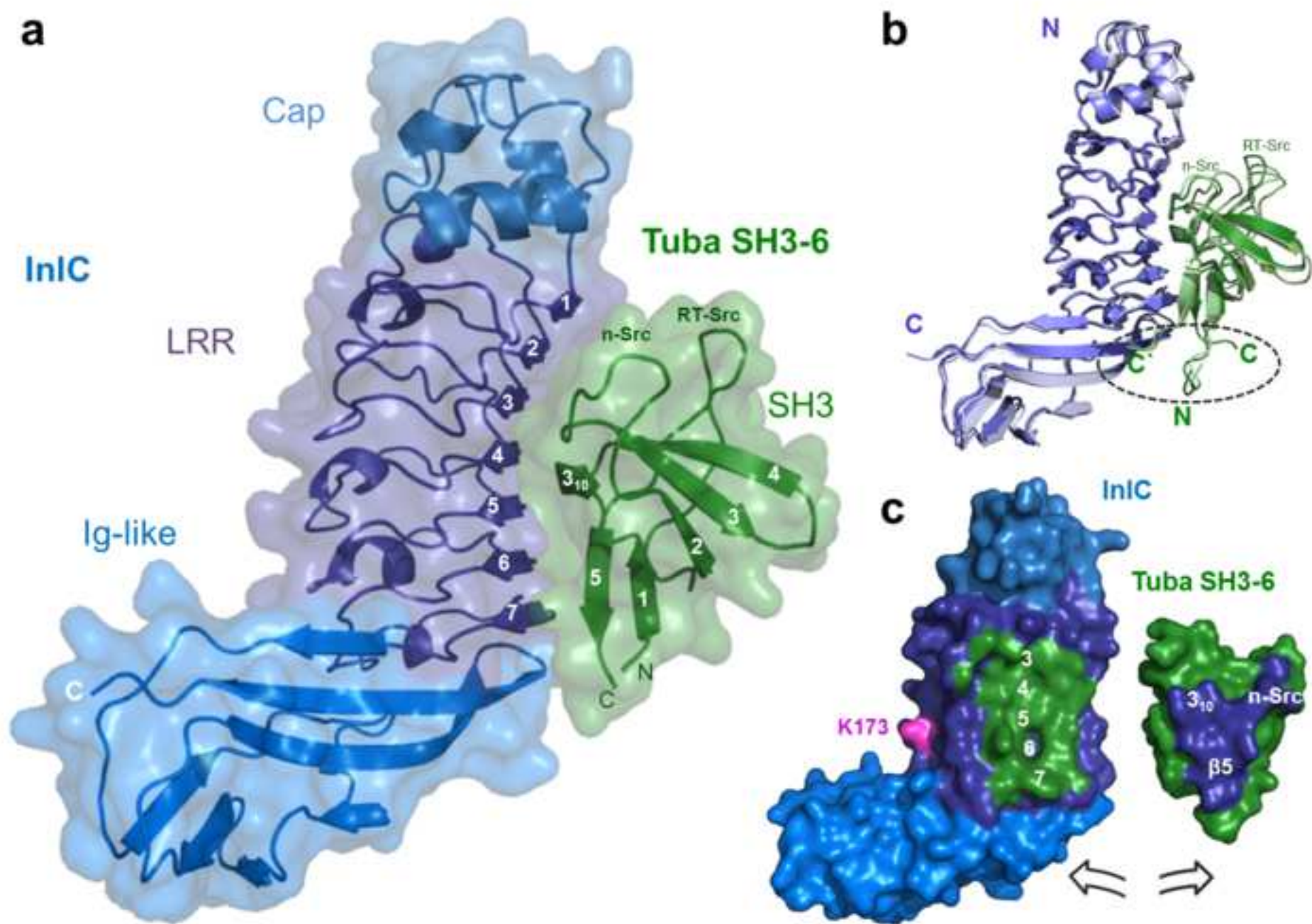
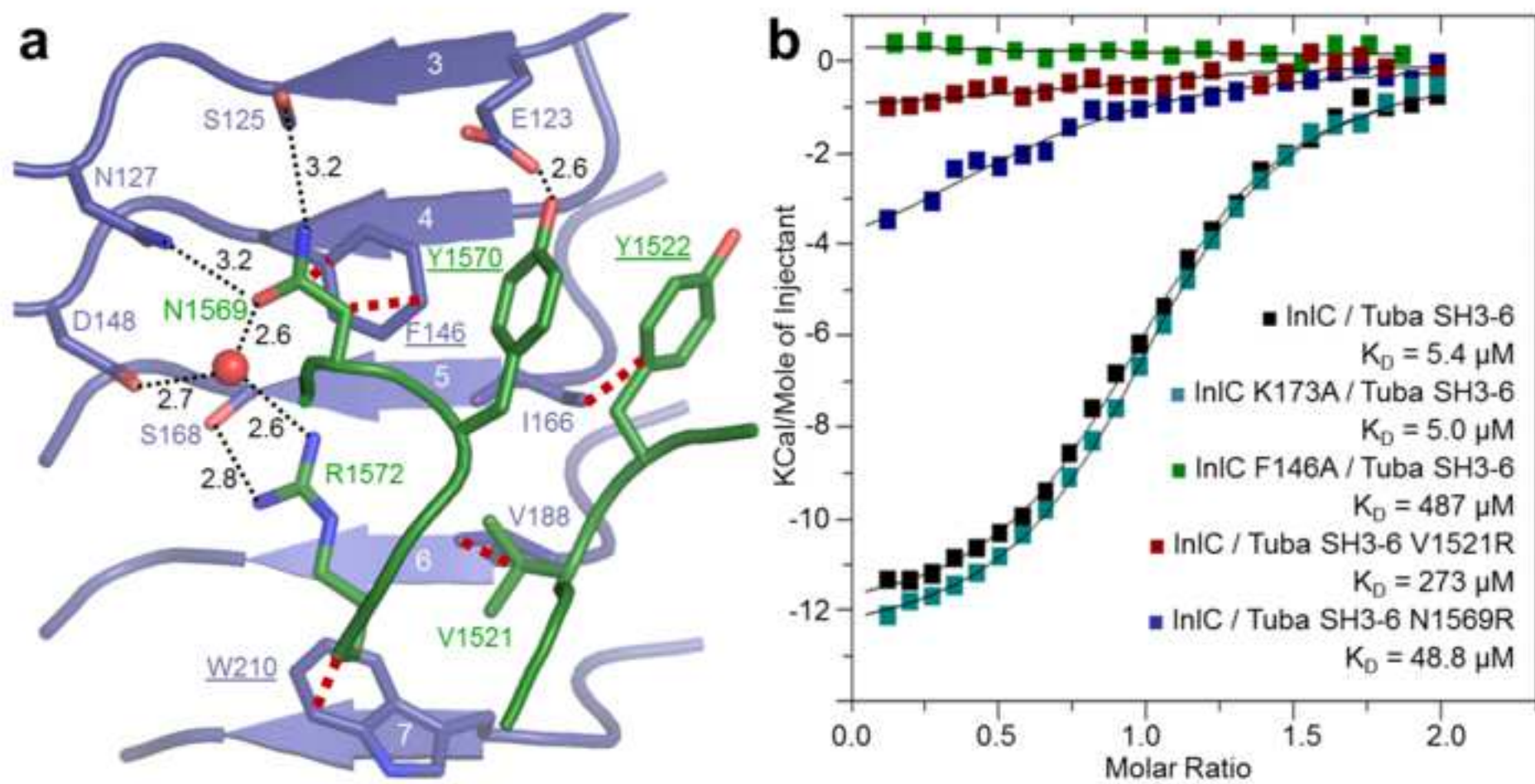


Figure 3
[Click here to download high resolution image](#)



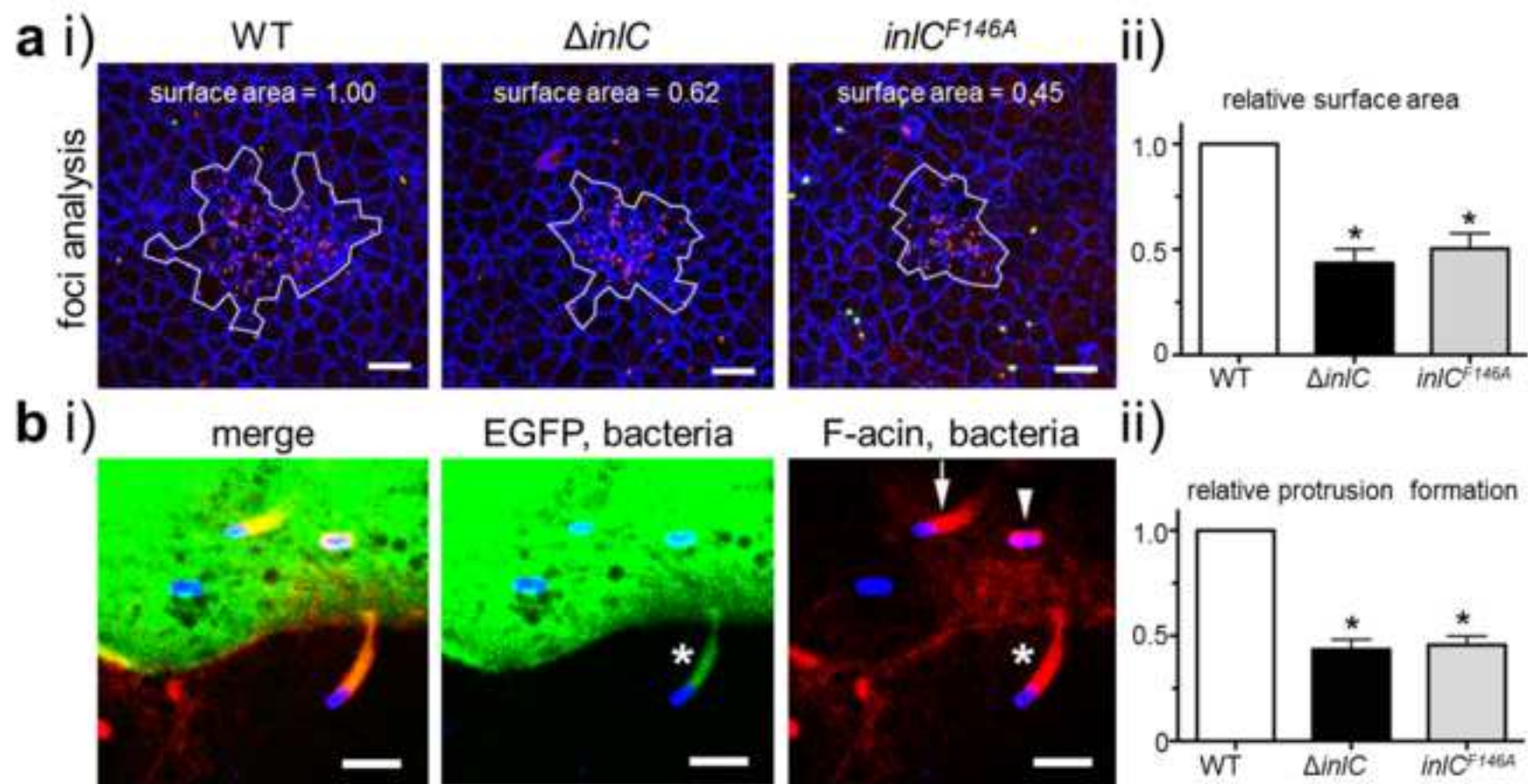


Figure 5

[Click here to download high resolution image](#)

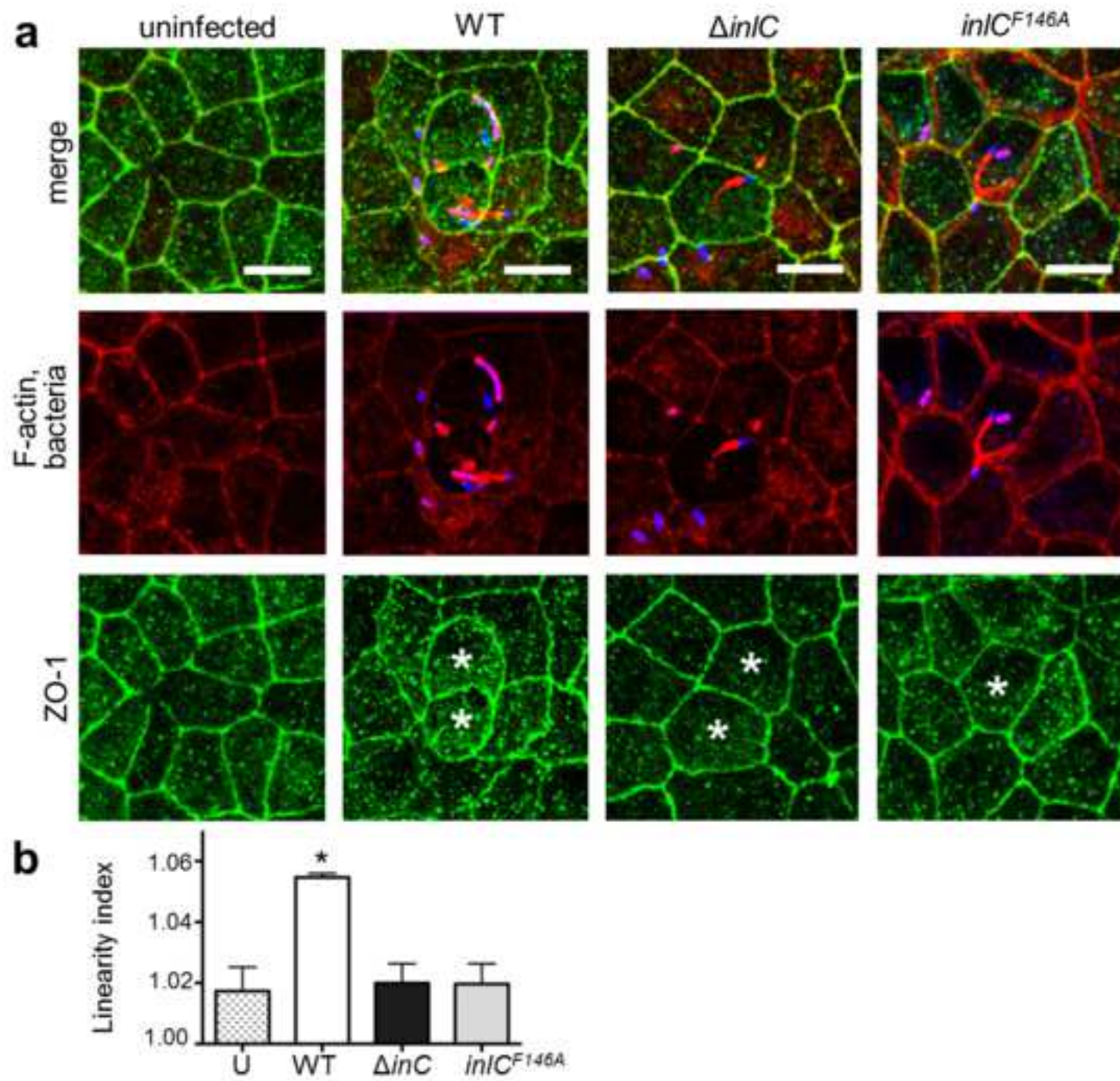
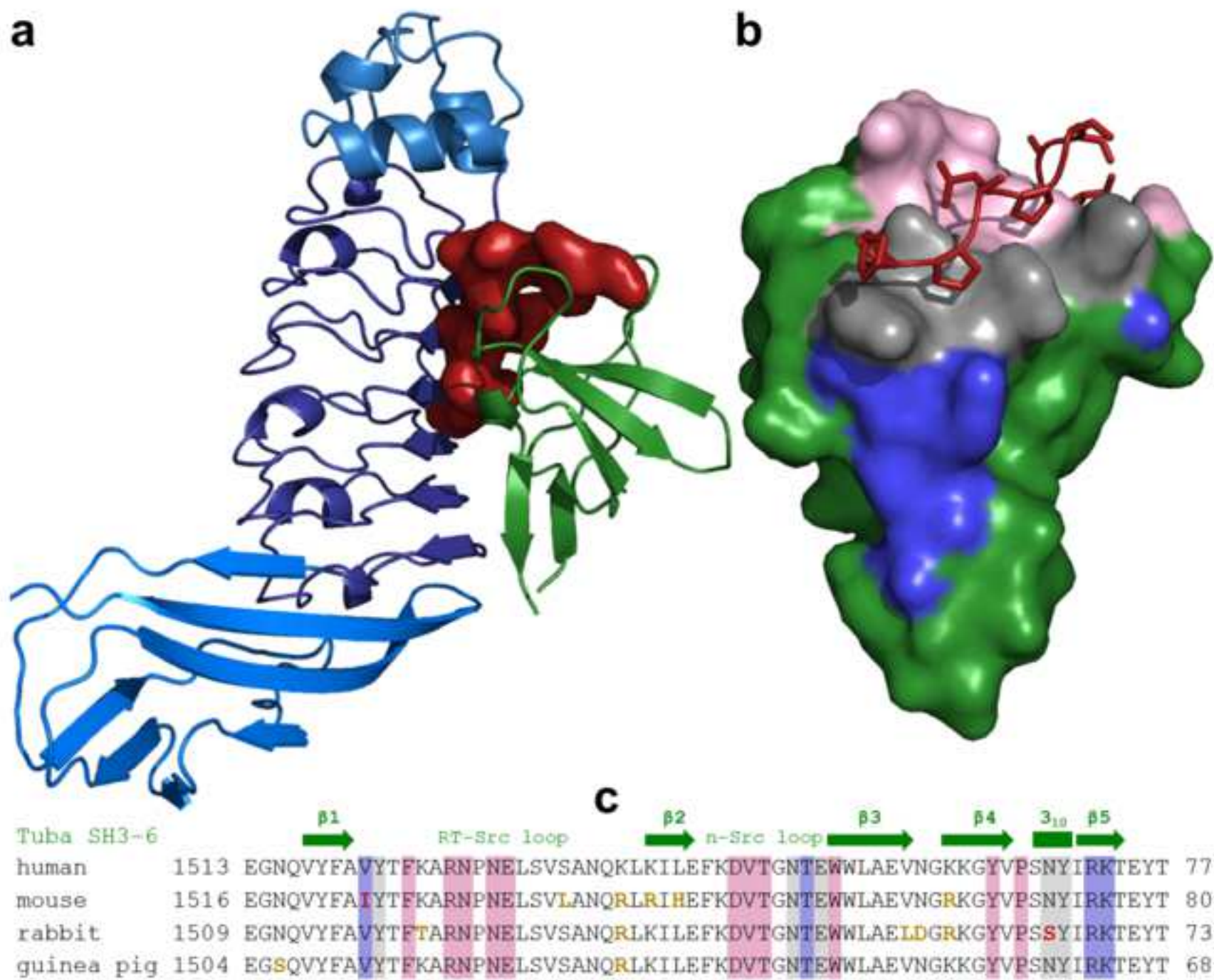


Figure 6
[Click here to download high resolution image](#)



Inventory of Supplemental Information

Figure S1 – Related to Figure 3. It provides qualitative binding data compared to quantitative Isothermal Titration Calorimetry data in Figure 3.

Figure S2 – Related to Figure 4. It serves to document levels of expression for the gene *inlC* in three strains of *Listeria monocytogenes*. This is a critical prerequisite for results shown in Figures 4 and 5.

Figure S3 – Related to Figure 4. It merely compares images prior and after interpretation.

Figure S4 – Related to Figure 6. It documents the occurrence of asymmetric Tuba SH3-6 dimers in three different crystal packing arrangements of this domain all in complex with proline-rich peptides.

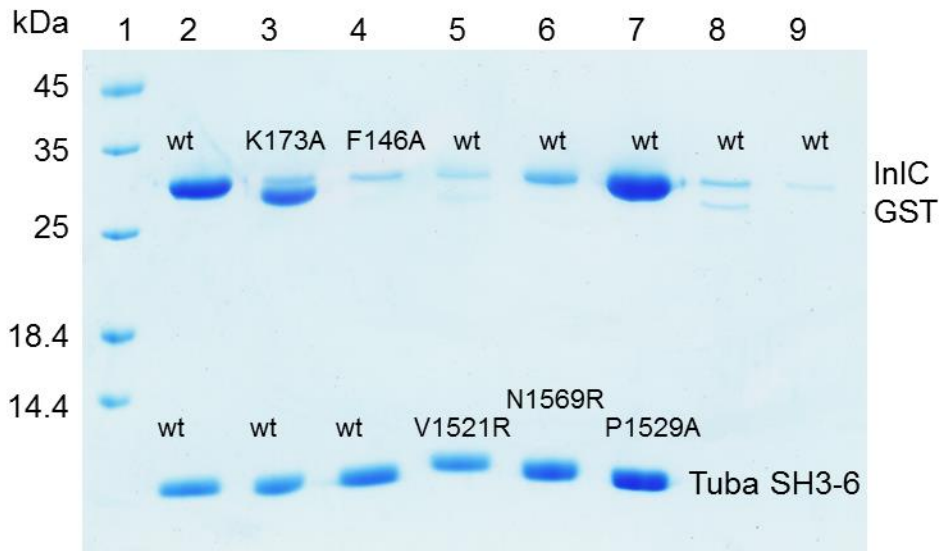
Figure S5 – Related to Figure 6. It documents the occurrence of Tuba SH3-6 oligomers in size exclusion chromatography experiments.

Table S1 – Related to the Experimental Procedures section and lists all DNA primers used for mutagenesis.

Table S2 – Related to Figure 3 and lists all interactions between InlC and Tuba SH3-6 – including interactions excluded from Figure 3 due to differences between three distinct complexes in the asymmetric unit.

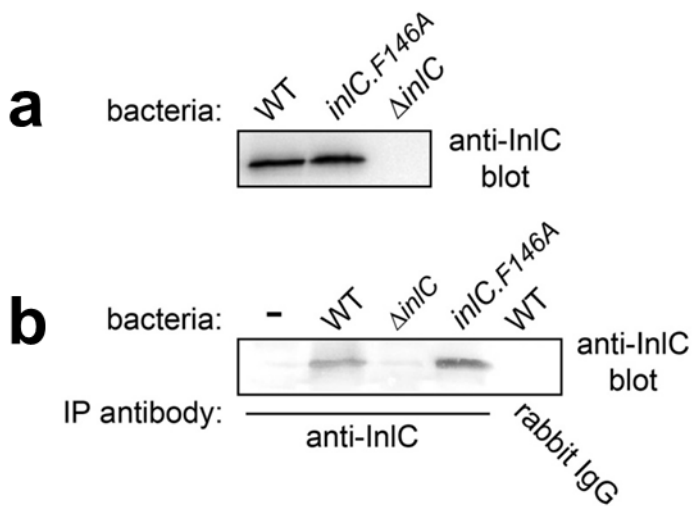
Supplemental Information

Figure S1: (Related to Figure 3)



InlC/Tuba SH3-6 interactions. GST-tagged Tuba SH3-6 wt or variants were bound to a glutathione agarose column. InlC wt or variants were added as indicated, incubated, unbound protein removed by washing, and any protein complex released by proteolytic cleavage. Lane 1 protein marker with molecular masses as indicated; Lane 2 InlC^{wt}/Tuba SH3-6^{wt} (1:1 complex); 3 InlC^{K173A}/Tuba SH3-6^{wt} (1:1); 4 InlC^{F146A}/Tuba SH3-6^{wt} (very weak binding); 5 InlC^{wt}/Tuba SH3-6^{V1521R} (very weak); 6 InlC^{wt}/Tuba SH3-6^{N1569R} (intermediate); 7 InlC^{wt}/Tuba SH3-6^{P1529A} (1:1); 8 and 9: controls for unspecific InlC binding to GST and glutathione agarose.

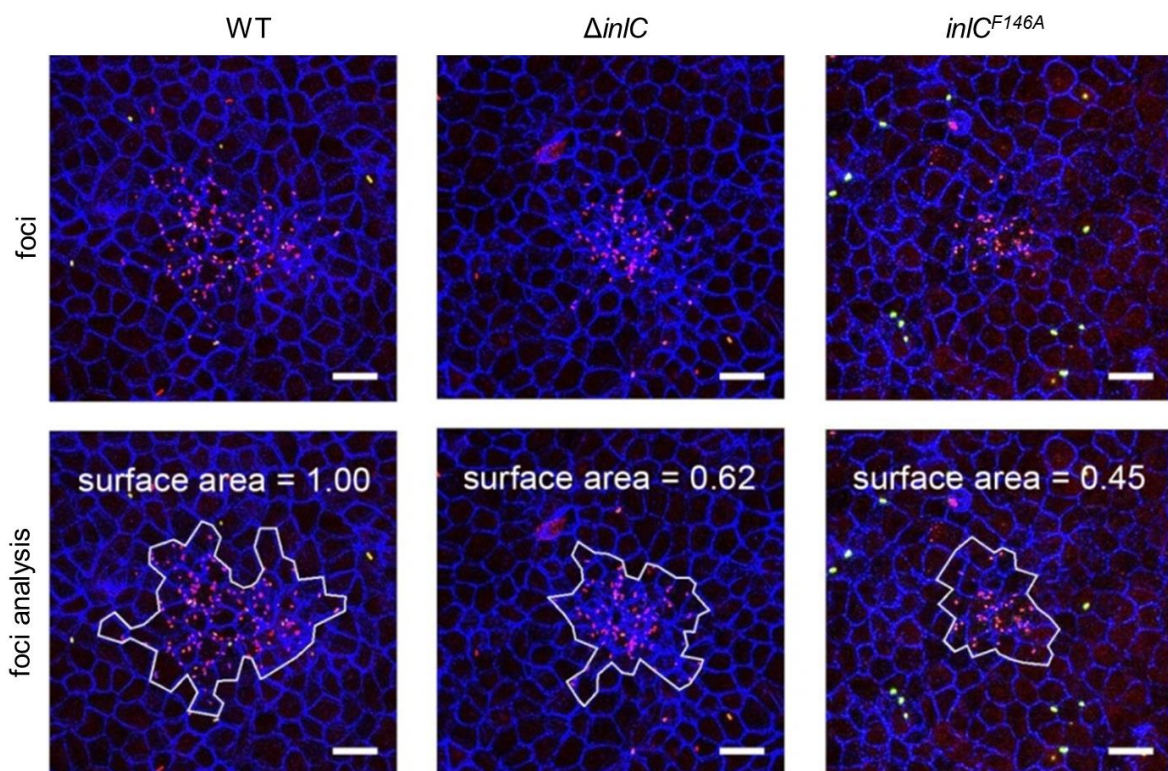
Figure S2: (Related to Figure 4)



Expression of the InlC^{F146A} mutant protein in *Lm*. An *Lm* mutant (*inlC^{F146A}*), expressing InlC with a phenylalanine-to-alanine substitution at amino acid 146, was constructed using site-directed mutagenesis and allelic replacement, as described in the Materials and Methods.

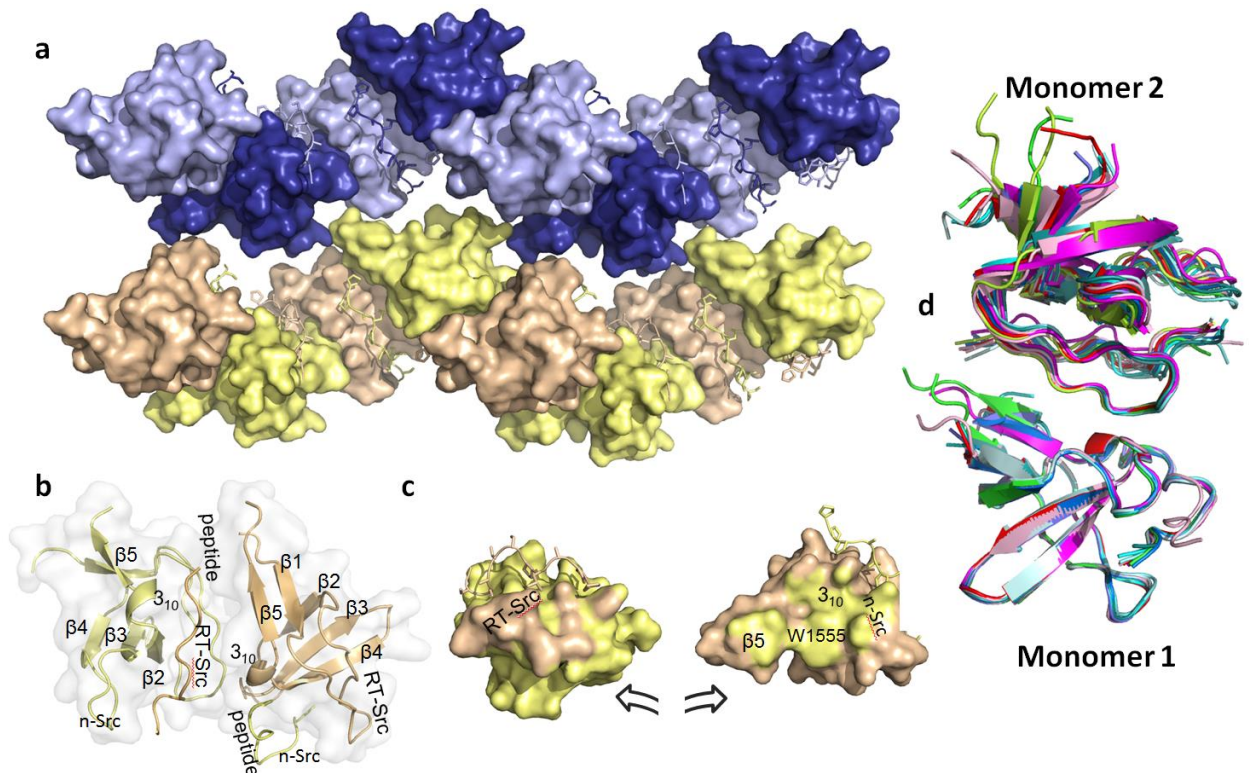
(a) Expression of InlC^{F146A} in broth culture. Overnight BHI broth culture supernatants of *inlC^{F146A}*, wild-type (WT) or *inlC* deletion ($\Delta inlC$) *Lm* strains were Western blotted using polyclonal anti-InlC antibodies. (b) Expression of InlC in infected human cells. Caco-2 BBE1 cells grown in transwells were infected with the indicated bacterial strains for 5.5 h, followed by solubilization of cells and immunoprecipitation of InlC. InlC proteins were detected by Western blotting of immunoprecipitates with anti-InlC antibodies.

Figure S3: (Related to Figure 4)



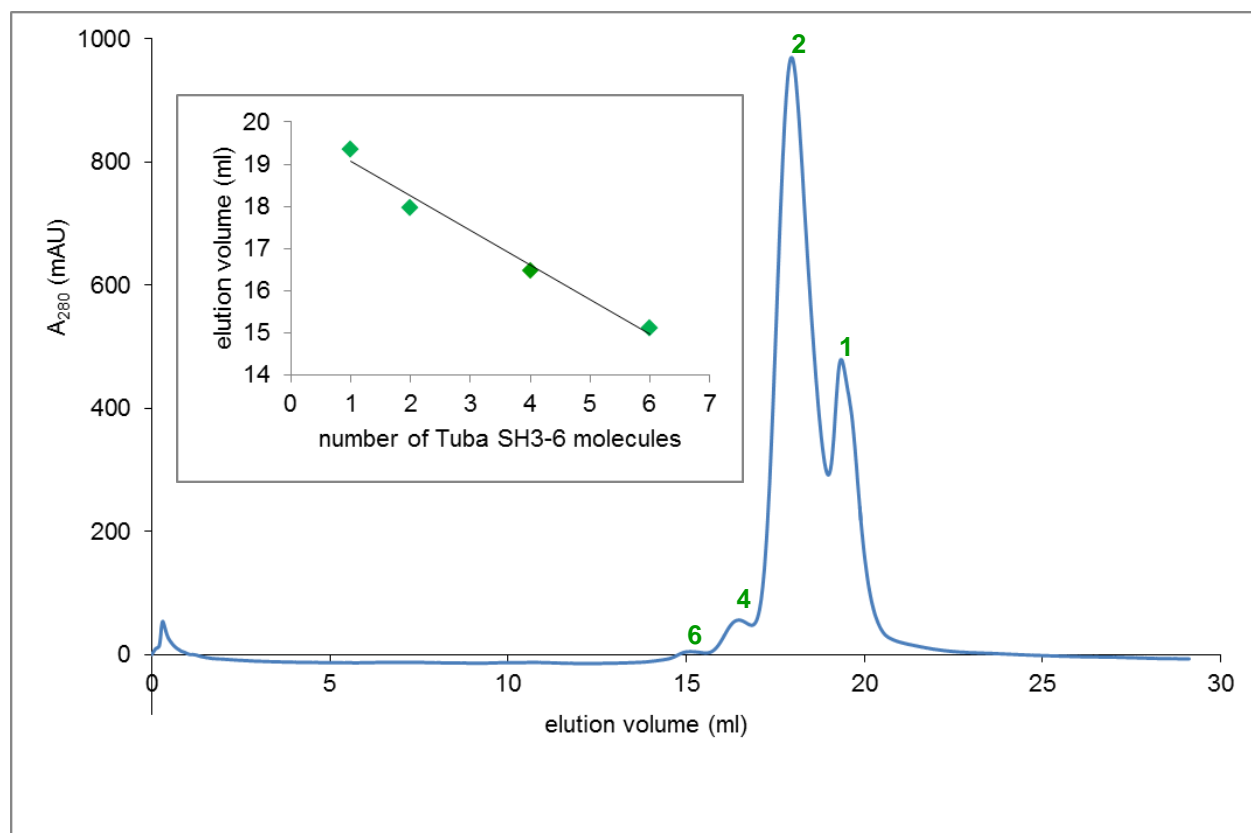
Foci of cell-cell spread of WT, $\Delta inlC$ and $inlC^{F146A}$ *Lm* strains in Caco-2 BBE1 cells as shown in Figure 4 A but prior to and following focal analysis.

Figure S4: (Related to Figure 6)



Asymmetric Tuba SH3-6 dimers in Tuba SH3-6/N-WASP peptide complexes in the $P2_12_12_1$ crystal packing. (a) Two helical SH36 fibers permeating Tuba SH3-6/N-WASP crystals based on repeating asymmetric Tuba SH3-6/N-WASP interactions. (b) Two Tuba SH3-6 domains forming an asymmetric dimer. The secondary structure is indicated. (c) Open-book surface representation of Tuba SH3-6 dimers interaction in B. Surface areas in contact with the partner protein adopt its color. The important parts involved in the interaction are labeled. (d) Structural alignment of 12 symmetrically independent Tuba SH3-6 dimers based on the bottom monomer (shades of green for two dimers from Tuba/N-WASP $P2_12_12_1$, blue for six dimers from Tuba/N-WASP $P4_1$ and magenta for four dimers from Tuba/Mena). The position and orientation of the second monomer is essentially invariant with minimal variation immediately adjacent to the first monomer but slight rotational adjustments with increasing distance from monomer 1.

Figure S5: (Related to Figure 6)



Size exclusion chromatography of Tuba SH3-6 domain demonstrating the oligomerization states. Main panel: The largest peak (marked 2, elution volume 18 ml), appears to represent Tuba SH3-6 dimers, the second largest peak (1, 19.4 ml) Tuba SH3-6 monomers. Significantly smaller peaks are observed for presumed tetramers (4, 16.5 ml) and hexamers (6, 15.2 ml). Insert: Plotting the elution volume of the assumed monomers, dimers, tetramers and hexamers against their oligomerization state, yields an approximate inverse relationship.

Table S1: Primers for QuickChange mutagenesis experiments (Related to Experimental Procedures)

Variant	Direction	Primer
InIC ^{Y246A-Y247A}	Forward	5'-GACCCAGATGGAAGATGGATATCTCCAGCTGC-CATCAGTAATGGTGGGAG-3'
	Reverse	5'-CTCCCACCATTACTGATGGCAGCTGGAGATATC-CATCTTCCATCTGGGTC-3'
InIC ^{F146A}	Forward	5'-GTGCTTGTTTATCTCGCTTGGCTTTAGATAACAA-CGAACTCAGAG-3'
	Reverse	5'-CTCTGAGTTCGTTGTTATCTAAAGCCAAGCGAG-ATAAACAAGCAC-3'
Tuba Δ7 SH3-6*	Forward	5'-CTGTTCCAGGGGCCCGAAGGCAACCAGGTC-3'
	Reverse	5'-GACCTGGTTGCCTTCGGGCCCTGGAACAG -3'
Tuba SH3-6 ^{V1521R}	Forward	5'-GGCAACCAGGTCTATTTGCTCGCTACACCTTC-AAGGCACG-3'
	Reverse	5'-CGTGCCTTGAAGGTGTAGCGAGCAAAATAGACC-TGGTTGCC-3'
Tuba SH3-6 ^{P1529A}	Forward	5'- CAAGGCACGAAACGCAAATGAGCTGAGCGTGTC -3'
	Reverse	5'- GACACGCTCAGCTCATTGCGTTTCGTGCCTTG -3'
Tuba SH3-6 ^{N1569R}	Forward	5'-GGGCTACGTTCCCTCCCGTTATATCCGCAAAACCG-3'
	Reverse	5'-CGGTTTTGCGGATATAACGGGAGGGAACGTAGCCC -3'
Lmo inIC ^{F146A}	Forward	5'- GTTTATCTCGCTTGGCATTAGATAACAACGAAC -3'
	Reverse	5'- GTTCGTTGTTATCTAATGCCAAGCGAGATAAAC -3'

*deletion of seven N-terminal residues

Table S2: InlC/Tuba SH3-6 interactions (Related to Figure 3)

InlC residue atom	Tuba residue atom	Water molecules in complex 1 / 2 / 3	Distance in complex 1 / 2 / 3 (Å)	Interaction Type
Invariant interactions (observed in all three complexes)				
Phe146	Asn1569		3.5 / 3.8 / 3.6	π
Ser125 O γ	Asn1569 N δ 2		3.2 / 3.2 / 3.7	HB
Asn127 N δ 2	Asn1569 O δ 1		3.2 / 3.5 / 3.1	HB
	Asn1569 N δ 2	W38/W78/W49	2.6 / 2.8 / 2.8	HB
Asp148 O δ		W38/W78/W49	2.7 / 2.8 / 2.8	HB
Asp148 O δ		W38/W78/W49	2.6 / 2.9 / 2.7	HB
Ser168 O γ	Arg1572 N η 2		2.8 / 2.9 / 2.7	HB
Trp210 C η 2	Arg1572 C β		3.5 / 3.4 / 3.3	vdW
Glu123 O ϵ 1	Tyr1570 O η		2.6 / 3.1 / 2.4	HB
Ile166 C δ 1	Tyr1522 C β		3.9 / 4.0 / 3.6	vdW
Val188 C γ 1	Val1521 C γ 2		4.2 / 3.9 / 4.0	vdW
Val188 C γ 2	Val1521 C β		4.2 / 4.0 / 4.1	vdW
Semi-variant interactions (observed in two of three complexes)				
Arg144	Tyr1522		3.3 / - / 3.3	π
Trp210 C ζ 2	Val1521 C γ 1		- / 3.7 / 3.9	vdW
Trp210 N ϵ 1		- /W3/W25	- / 3.1 / 3.0	HB
Asp212 O δ 2		- /W3/W25	- / 2.6 / 2.7	HB
	Lys1573 O	- /W5/W36	- / 2.8 / 2.8	HB
Ser105 O γ	Glu1553 O ϵ 1		3.0 / - / 3.3	HB
Asn127 N δ 2	Glu1553 O ϵ 1		2.6 / - / 2.7	HB
Arg170 N η 2	Glu1575 O ϵ 2		- / 3.5 / 2.8	SB
Arg170 N η 1	Glu1575 O ϵ 1		- / 3.1 / 3.3	SB
Asp190 O δ 2	Arg1572 N η 2		2.5 / - / 2.8	SB
His192	Glu1575		- / 3.2 / 2.8	π
Minority interactions (observed in one of three complexes)				
Asn84 N δ 2		W138/ - / -	3.1 / - / -	HB
Ile166 C γ 2	Tyr1522		- / 3.5 / -	CH.. π
Arg128 N η 1	Thr1552 O γ 1		- / - / 2.7	HB
Arg170	Arg1572		3.5 / - / -	π
Asp190 O δ 2	Arg1572 N ϵ		- / 2.8 / -	SB
	Lys1573 N	- /W5/W36	- / - / 3.0	HB
	Asn1551 O δ 1	W138/ - / -	2.4 / - / n/a	HB

HB: Hydrogen bond; SB: Salt bridge; vdW: van der Waals interaction; π : π -stacking
Complex 1: Chains A and B; complex 2: chains C and D; complex 3: chains E and F

Polle *et al* reveal the atomic details of InIC from *Listeria monocytogenes* targeting the sixth SH3 domain of human Tuba to interrupt its physiological interaction with N-WASP. The bacterium thereby locally interferes with cortical actin tension enabling it to deform the cell membrane and infect neighboring uninfected cells via protrusions.